

Relativistic R -matrix close-coupling method based on the effective many-body Hamiltonian: Benchmarks on the electron-impact excitations of the Kr^{6+} ion

Yasuyuki Ishikawa*

Department of Chemistry and the Chemical Physics Program, University of Puerto Rico,
P.O. Box 23346 San Juan, Puerto Rico 00931-3346, USA

Marius J. Vilkas

College of Pharmacy, University of Kentucky, 725 Rose Street, Lexington, Kentucky 40508, USA

(Received 27 October 2007; published 2 May 2008)

A relativistic R -matrix close-coupling method based on effective many-body Hamiltonians is employed to calculate the electron-impact excitations of intercombination transitions in the Kr^{6+} ion as benchmarks in the quest for accurate representation of the target and collisional states in multivalence-electron ions. The effective Hamiltonian in relativistic multireference many-body perturbation theory accurately accounts for short-range many-body interactions unaccounted for by limited configuration-interaction representations of the basis states. The R -matrix method is successfully applied to the near-threshold electron impact excitation of the $4s^2\ ^1S \rightarrow 4s4p\ ^3P$ intercombination transition in the zinlike krypton (Kr^{6+}) ion, where the observed disagreement between the experimental absolute total cross sections dominated by dielectronic resonances and those predicted by using the Breit-Pauli and Dirac R -matrix methods reveals an inadequacy of the extant R -matrix close-coupling calculations in compact configuration-interaction representation of target states.

DOI: [10.1103/PhysRevA.77.052701](https://doi.org/10.1103/PhysRevA.77.052701)

PACS number(s): 34.80.Dp, 31.15.A-, 31.15.xp, 31.15.xr

I. INTRODUCTION

Electron-atomic-ion collision is a fundamental process in astrophysical and laboratory plasmas [1,2]. Of particular importance is the electron-impact excitation of atomic ions since accurate predictions form the basis of plasma temperature and density diagnostics [1,3–5]. Recent energy-loss merged electron-ion beams [6–8] and electron-beam ion trap (EBIT) experiments [9,10] for measuring differential and total cross sections have provided important experimental benchmarks for theoretical methods employed to calculate electron-ion excitation processes. Among these methods, the R -matrix version of the close coupling (CC) theory is the most efficient and successful for simulating low-energy collision processes [11–24]. Theoretical calculations of electron-impact excitations must provide the large amount of data needed to interpret laboratory and astrophysical plasmas. The role of the precious electron-impact excitation experiments is to provide a benchmark by which to compare the levels of accuracy of the theoretical methods [6].

Experimental measurements of total cross sections for electron-impact excitations of a state involving a change of electron spin are still a rarity in atomic physics [6,7,9]. Bannister *et al.* [6] reported the first measurements of absolute total cross sections for such a collision, the near-threshold electron impact excitation of the $4s^2\ ^1S \rightarrow 4s4p\ ^3P$ intercombination transition in Kr^{6+} , which is dominated by strong near-threshold dielectronic resonances. The electron impact excitation of the intercombination transition is significantly more complicated than any of the systems previously studied because the large number of core electrons, particularly a full $3d$ core, with two valence electrons, makes it extremely dif-

ficult to accurately describe the target and resonance states [25]. These target and resonance levels have large level shifts due to relativistic many-body effects, which must be fully incorporated to account for the nearly 1 eV fine structure splitting between the $4s4p\ ^3P_{2,1,0}^o$ as well as other excited levels. Extant many-body methods cannot adequately address the problem of several electrons in the valence shell [26]. Consequently, fully converged results for this resonance process have not been achieved to date, even with the use of the Breit-Pauli and Dirac Hamiltonians in the R -matrix CC calculations [25].

Electron impact excitations in multivalence-electron ions, such as those of the intercombination transition in Kr^{6+} , serve as benchmarks in the quest for a higher level of theory for high-accuracy cross-section calculations, and therefore present an important testing ground for the development of electron-atom collision theory. The need for accurate prediction of electron-impact excitation cross sections and apparent differences between experiment and extant theoretical predictions for multielectron ions warrant continued theoretical refinement [27,28]. In particular, improved calculations require accurate treatment of the short-range many-body interaction [27], or dynamic correlation, along with relativity with high-accuracy relativistic many-body theories [29–34]. Building on our earlier successes in highly accurate relativistic many-body calculations for the spectra of multivalence-electron systems [26,35], we have generalized the Dirac R -matrix algorithm [12,36,37], and developed a relativistic R -matrix CC method based on our relativistic multireference many-body perturbation theory (MR-MBPT) [38]. The method accurately accounts for static and dynamic correlations, and thus enables accurate prediction of the electron impact excitations, including the effects of resonances, channel coupling, and relativity. The unification of the relativistic MR-MBPT and R -matrix CC theories addresses the problem

*yishikawa@uprrp.edu

of electron-atom collision processes that follows the earlier success of our relativistic many-body perturbation theory [26,35] for atomic structure and spectroscopy.

In the present study, the recently developed relativistic R -matrix CC method, based on the effective many-body Hamiltonians [38] for accurate representation of the N -electron target and $(N+1)$ -electron scattering Hamiltonian matrices, is applied to the electron impact excitation of $4s^2\ ^1S \rightarrow 4s4p\ ^3P_{2,1,0}^o$ intercombination transition in Kr^{6+} in order to assess the accuracy of the theory. The method is successfully applied to benchmark measurement of the near-threshold electron impact excitation, where experimental absolute total cross sections [6] have not satisfactorily matched those from the extant R -matrix close-coupling calculations in compact configuration-interaction (CI) representation of target states. A primary goal of this study is to provide many-body theoretical underpinnings for accurate description of electron-impact excitation processes.

II. METHOD

To obtain an explicit expression for scattering amplitude and cross section, the CC approximation employs a CI expansion for the $(N+1)$ -electron wave function of collision system (N -electron target plus incident electron), in which those states most strongly coupled to the initial and final states are included in the finite expansion. If the configuration space is partitioned into two regions separated by the R -matrix boundary R_a , the total scattering wave function for the $(N+1)$ -electron collision complex in the internal region may be expressed as

$$\Psi_K^{N+1} = \sum_{ij} c_{ijK} \mathcal{A}[\Psi_i^N, u_{ij}] + \sum_{q=1} d_{qK} \theta_q^{N+1}, \quad (1)$$

where Ψ_i^N is the wave function of the N -electron target state i , $\{u_{ij}\}$ is the R -matrix basis for the scattering electron, and $\{\theta_q^{N+1}; q=1, 2, \dots, M_\theta\}$ is a set of square-integrable functions that represent the bound channels constructed by adding a valence electron to the target states. The $\{\theta_q^{N+1}\}$ are also referred to as the correlation functions, included to compensate for loss when the orthogonality with bound spinors of $\{u_{ij}\}$ is imposed and to add some short-range many-body effects [22,41]. The $\{\Psi_i^N\}$, $\{\theta_q^{N+1}\}$, and R -matrix basis $\{u_{ij}\}$ are constructed from bound and free Dirac four-spinors. The boundary is chosen so that the magnitude of the radial spinors of the bound electrons of the target is vanishingly small and exchange between incident electron and target electrons outside the R -matrix sphere is negligible. The coefficients c_{ijK} and d_{qK} are determined variationally, by diagonalizing the $(N+1)$ -electron Hamiltonian H^{N+1} matrix in the R -matrix close-coupling theory,

$$H_{KK'}^{N+1} = \langle \Psi_K^{N+1} | H^{N+1} | \Psi_{K'}^{N+1} \rangle. \quad (2)$$

The N - and $(N+1)$ -electron Hamiltonians (in atomic units) for the development of our relativistic R -matrix algorithm is taken to be the so-called no-pair Dirac-Coulomb-Breit (DCB) Hamiltonian [39,40]

$$H_{DCB}^\eta = \sum_i^\eta h_D(i) + \mathcal{L} \sum_{i>j}^\eta \left[\frac{1}{r_{ij}} + B_{ij}(0) \right] \mathcal{L} \quad (3)$$

with $B_{ij}(0)$ the frequency-independent Breit interaction. Here $h_D(i)$ is the Dirac one-electron Hamiltonian, $\eta=N$ and $N+1$, respectively, for the N - and $(N+1)$ -electron systems, and \mathcal{L} is a projection operator onto the positive energy space spanned by the N -electron configuration-state functions (CSFs) constructed from the positive-energy eigenfunctions of the Dirac-Fock self-consistent field (SCF) equation [40].

A. Effective Hamiltonian for accurate representation of the target states

In the extant R -matrix CC expansion [Eq. (1)], the N -electron target wave function Ψ_i^N is approximated by a finite CI expansion in the multielectron CSFs. Unless a large-scale expansion is employed, the CI representation of the N -electron target states fails to account for the bulk of dynamic correlation [26]. The residual dynamic correlation corrections unaccounted for in the CI expansion constitute a significant fraction of the theory-experiment deviation in the excitation and ionization energies. In this subsection, an effective Hamiltonian in the relativistic MR-MBPT for the N -electron target states is introduced to correct for the residual dynamic correlation in the CI representation of the target wave function.

In order to account for strong configuration mixing among the ground and excited levels, the multireference configuration interaction method (MR-CI) is introduced in an extended subspace $\mathfrak{P}_{CI}^{(+)}$ of positive-energy space. N -electron eigenfunctions of the no-pair DCB Hamiltonian are approximated by a linear combination of M_{CI} configuration-state functions, $\{\Phi_I^{(+)}(\gamma_I \mathcal{J} \pi); I=1, 2, \dots, M_{CI}\} \in \mathfrak{P}_{CI}^{(+)}$, constructed from the one-particle positive-energy spinors computed in matrix multiconfigurational Dirac-Fock self-consistent field calculations [34]. Varying the configuration-state coefficients $\{C_{IK}\}$ leads to the determinantal CI equation. The eigenfunctions $\{\psi_K^{CI}(\gamma_K \mathcal{J} \pi)\}$ of the CI equation form a subspace $\mathfrak{P}_{CI}^{(+)}$ of the positive-energy space $\mathfrak{D}^{(+)}$. The frequency-dependent Breit interaction, normal mass shift (NMS), and specific mass shift (SMS) are evaluated as the first-order corrections using the eigenvectors $\{\psi_K^{CI}(\gamma_K \mathcal{J} \pi)\}$ from the MR-CI.

The N -electron DCB Hamiltonian H_{DCB}^N is decomposed into two parts, unperturbed Hamiltonian H_0^N and perturbation V , following Møller and Plesset [42,43],

$$H_{DCB}^N = H_0^N + V. \quad (4)$$

The subset, $\{\Phi_I^{(+)}(\gamma_I \mathcal{J} \pi); I=1, 2, \dots, M_{CI}\} \in \mathfrak{P}_{CI}^{(+)}$, with which we expand the CI wave function $\psi_K^{CI}(\gamma_K \mathcal{J} \pi)$, defines an active subspace $\mathfrak{P}_{CI}^{(+)}$ spanned by $\psi_K^{CI}(\gamma_K \mathcal{J} \pi)$ and its $M_{CI} - 1$ orthogonal complements, $\{\psi_K^{CI}(\gamma_K \mathcal{J} \pi); K=1, 2, \dots, M_{CI}\}$. The residual space in the positive-energy subspace is $\mathfrak{D}^{(+)} = \mathfrak{D}^{(+)} - \mathfrak{P}_{CI}^{(+)}$, which is spanned by CSFs $\{\Phi_L^{(+)}(\gamma_L \mathcal{J} \pi); L=M_{CI}+1, M_{CI}+2, \dots\}$.

Application of the Rayleigh-Schrödinger perturbation theory provides order-by-order expressions of the perturbation series. The matrix elements of the effective Hamiltonian up to the first-order may now be expressed as

$$(H_{eff}^{(0+1)N})_{IJ} = \langle \Phi_I^{(+)}(\gamma_I \mathcal{J} \pi) | H_{DCB}^N | \Phi_J^{(+)}(\gamma_J \mathcal{J} \pi) \rangle; \quad (5)$$

$$I, J = 1, 2, \dots, M_{CI},$$

with the eigenfunctions $\Psi_{CI}^{CI}(\in \mathfrak{R}^{(+)}) = \sum_{I=1}^{M_{CI}} C_{KI}^{CI} \Phi_I^{(+)}$ and eigenvalue $E_K^{(0+1)} (= E_K^{CI})$. The matrix elements of the second-order term in the effective Hamiltonian may also be expressed as

$$(H_{eff}^{(2)N})_{IJ} = \sum_{L=M_{CI}+1}^{\mathcal{D}^{(+)}} \frac{\langle \Phi_I^{(+)} | V | \Phi_L^{(+)} \rangle \langle \Phi_L^{(+)} | V | \Phi_J^{(+)} \rangle}{E_J^{CSF} - E_L^{CSF}}. \quad (6)$$

The eigenvalue equation for the N -electron target states may be expressed as

$$(H_{eff}^{(0+1)N} + \mathcal{H}_{eff}^{(2)N}) \Psi_K^{N,eff} = E_K^{(0+1+2)} \Psi_K^{N,eff}. \quad (7)$$

Here $\Psi_K^{N,eff}$ are the eigenvectors of the effective Hamiltonian, and $(\mathcal{H}_{eff}^{(2)N})_{IJ} = 1/2[(H_{eff}^{(2)N})_{IJ} + (H_{eff}^{(2)N})_{JI}]$, which is Hermitian [44]. The eigenstates of the effective Hamiltonian are employed for the target description in the CC expansion [Eq. (1)]. The intermediate coupling is naturally accounted for in the MR-MBPT to construct the effective Hamiltonian.

B. Effective Hamiltonian for $(N+1)$ -electron collisional system

To construct the effective Hamiltonian for the collisional system, the $(N+1)$ -electron configuration space is partitioned into two manifolds: the bound-channel manifold of CSFs $\{\theta_q^{N+1}; q=1, 2, \dots, M_\theta\}$ and scattering-channel manifold $\{\mathcal{A}[\Psi_i^{eff}, u_{ij}]\}$. Then the $(N+1)$ -electron effective Hamiltonian can be written in matrix form,

$$H_{KK'}^{N+1} = \begin{pmatrix} H_{bb} & H_{bc} \\ H_{cb} & H_{cc} \end{pmatrix}. \quad (8)$$

Following the same procedure described in the previous section, the bound-bound H_{bb} block of the $(N+1)$ -electron effective Hamiltonian can be expressed by its matrix elements:

$$(H_{bb})_{qq'} = \langle \theta_q^{N+1} | H_{DCB}^{N+1} | \theta_{q'}^{N+1} \rangle + \sum_{L=M_{q+1}} \frac{\langle \theta_q^{N+1} | V | \theta_L^{N+1} \rangle \langle \theta_L^{N+1} | V | \theta_{q'}^{N+1} \rangle}{E_q^{CSF} - E_L^{CSF}}. \quad (9)$$

The off-diagonal block H_{bc} involving the target state is expressed in terms of the eigenfunctions Ψ_K^{eff} of the N -electron target effective Hamiltonian,

$$(H_{bc})_{q[ij]} = \langle \theta_q^{N+1} | H_{DCB}^{N+1} \mathcal{A}[\Psi_i^{eff}, u_{ij}] \rangle. \quad (10)$$

The continuum-continuum block H_{cc} is expressed as

$$(H_{cc})_{[ij][i'j']} = \langle \mathcal{A}[\Psi_i^{eff}, u_{ij}] | H_{DCB}^{N+1} | \mathcal{A}[\Psi_{i'}^{eff}, u_{i'j'}] \rangle. \quad (11)$$

The diagonal matrix elements of the continuum-continuum block H_{cc} may be expressed in two parts. The first part contains only the energy contributions from the Dirac spinors of the bound electrons and is equal to the target state energy $E_i^{(0+1+2)}$ in this channel. The second part contains the remaining, one-electron integrals involving the R -matrix continuum basis spinors. Because of the weak interaction of the con-

tinuum electron with the target electrons, this part is nearly equal to the kinetic energy ε_{ij} of the scattering electron,

$$(H_{cc})_{[ij][ij]} = E_i^{(0+1+2)} + \varepsilon_{ij} + \Delta\varepsilon_{ij}. \quad (12)$$

Here $\Delta\varepsilon_{ij}$ represents the energy terms arising from the interaction of the continuum electron with target electrons. The crucial difference between the previous studies and the present reformulation lies in the description of the target and $(N+1)$ -electron collisional states by effective many-body Hamiltonians that accurately account for electron correlation. Accurate representations of the target states and bound channels are implemented using the effective Hamiltonians in relativistic MR-MBPT.

C. Computation

The large and small radial components of the bound Dirac spinors were expanded in sets of even-tempered Gaussian-type functions (GTFs) that satisfy the boundary conditions associated with the finite nucleus [45]. The GTFs that satisfy the boundary conditions associated with the finite nucleus are automatically kinetically balanced [45]. Even-tempered basis sets of $26s24p22d20f$ G spinors (G for ‘‘Gaussian’’) were employed for up to angular momentum $L=3$, 18 G spinors for $L=4-5$, and 15 G spinors for $L=6-11$. The order of the partial-wave expansion L_{\max} in second-order perturbation theory expansion [Eqs. (6) and (9)], the highest angular momentum of the spinors included in the virtual space, is $L_{\max}=11$. The nuclei were simulated as spheres of uniform proton charge with radii (bohr) $R=2.2677 \times 10^{-5} A^{1/3}$, where A (amu) is atomic mass.

The state-averaged MCDFB SCF procedure [26] for the ground and low-lying excited $J=0-3$ target states in the Zn-like ion was carried out optimizing the average of the energies of the 14 even- and odd-parity CSFs arising from the $4s^2$, $4s4p$, $4p^2$, and $4s4d$ configurations. Intermediate coupling is built in through the MCDFB SCF process. This single set of orthonormal spinors, determined by the MCDFB SCF, was subsequently employed to construct the CSFs for both the N -electron target and $(N+1)$ -electron collisional systems. Subsequent complete active space (CAS) CI included all the relativistic CSFs arising from the nonrelativistic configurations, $4s^m 4p^n 4d^p$ with $m+n+p=2$ of the $n=4$ manifold. A total of 35 CSFs of $J=0-4$, 19 even-parity and 16 odd-parity CSFs, thus produced were included in the CAS CI calculations, and each of the 35 eigenstates was subjected to additional refinement to account for the residual dynamic correlation by solving the 35×35 matrix eigenvalue equation of the effective Hamiltonian [Eq. (7)]. All electrons have been included in the MR-MBPT perturbation theory calculations to determine accurately the effects of relativity and electron correlation. Radiative corrections, the Lamb shifts, were estimated for each bound state by evaluating the electron self-energy and vacuum polarization following an approximation scheme, as discussed by Indelicato, Gorceix, and Desclaux [46].

The matrix elements of the H_{bb} and H_{bc} blocks of the $(N+1)$ -electron effective Hamiltonian were constructed with the bound channel functions $\{\theta_q^{N+1}; q=1, 2, \dots, M_\theta\}$ gener-

ated by adding a $n=4$ valence electron to all the target CSFs. This leads to the three valence-electron $n=4$ CAS configurations, $4s^m 4p^n 4d^p$ with $m+n+p=3$, for the bound channel. A total of 149 CAS CSFs of $J=1/2-11/2$, 72 even-parity and 77 odd-parity CSFs, thus produced, were included in the evaluation of the bound-bound H_{bb} block of $(N+1)$ -electron effective Hamiltonian matrix, with the MR-MBPT refinement accounting for the residual dynamic correlation.

To achieve accurate description of the low-energy electron-impact excitation processes using the effective Hamiltonian approach, the Dirac atomic R -matrix codes (DARC) [36] were significantly modified. A relatively small set of continuum basis $\{u_{ij}\}$ sufficed to describe low-energy scattering processes. We chose 35 continuum basis functions for each κ value of the continuum-electron angular momentum for the moderately large R -matrix boundary of 17.0 atomic units, where the valence spinors have vanishingly small amplitudes of $\approx 10^{-8}$. In our effective Hamiltonian approach, the R -matrix boundary is chosen for all target valence spinors to have vanishingly small amplitudes so that exchange and correlation effects are negligible outside the boundary. The Buttle correction is made as it is implemented in DARC.

III. RESULTS AND DISCUSSIONS

A. Term energies of the 30-electron target and 31-electron collisional systems

In Table I, the available experimental term energies compiled in the National Institute of Standards and Technology (NIST) Atomic Spectra Database [47] are compared with the effective many-body Hamiltonian and CAS CI calculations for the lowest 24 target states. The term energies computed by diagonalizing the 35×35 effective many-body Hamiltonian matrix deviate from experiment on the order of 100 cm^{-1} (0.01 eV). The effective Hamiltonian in relativistic MR-MBPT accurately accounts for nondynamic and dynamic correlations along with relativistic and QED effects, and yield the term energies with near spectroscopic accuracy. In marked contrast, the term energies computed by using the 35-CSF CAS CI deviate from experiment by up to $\approx 4000 \text{ cm}^{-1}$, rendering the CAS-CI R -matrix CC calculations inaccurate, because the CI fails to account for the bulk of dynamic correlations. A large-scale CI, including at least the $3d$ -electron excitations in CSFs, would be necessary to correct for the missing dynamical correlation and improve the description of the term energies. The results underscore the importance of treating the valence-core correlation with the MR-MBPT term [Eq. (6)] in the effective Hamiltonian for achieving the near spectroscopic accuracy.

In Table II, available experimental term energies for the lowest 36 levels in Kr^{5+} are compared with those calculated by using the 148-CSF CAS CI and the effective many-body Hamiltonian methods. The deviation from experiment of the CAS CI energies reaches up to 5000 cm^{-1} (0.6 eV). The term energies calculated with the effective many-body Hamiltonian deviate from experiment on the order of 100 cm^{-1} for most of excited levels. The experimental energy levels that deviate from theory by more than 1000 cm^{-1}

TABLE I. Comparison with experiment [47] of the calculated term energies (cm^{-1}) of zinlike Kr (Kr^{6+}). Percentage deviations from the experimental values are given in parentheses.

State	Expt.	CAS-CI	MR-MBPT
$4s^2 \ ^1S_0$	0	0(0.00)	0(0.00)
$4s4p \ ^3P_0^o$	117390	113344(3.45)	117768(0.32)
$4s4p \ ^3P_1^o$	120095	116052(3.37)	120484(0.32)
$4s4p \ ^3P_2^o$	126553	122307(3.36)	126951(0.31)
$4s4p \ ^1P_1^o$	170835	174197(1.97)	170455(0.22)
$4p^2 \ ^3P_0$	274932	272801(0.78)	275131(0.07)
$4p^2 \ ^3P_1$	279414	276929(0.89)	279615(0.07)
$4p^2 \ ^3P_2$	288190	284866(1.15)	288446(0.09)
$4p^2 \ ^1D_2$	279715	275945(1.35)	280360(0.23)
$4p^2 \ ^1S_0$	321794	325719(1.22)	322768(0.30)
$4s4d \ ^3D_1$	349973	346229(1.07)	350384(0.12)
$4s4d \ ^3D_2$	350417	346684(1.07)	350843(0.12)
$4s4d \ ^3D_3$	351116	347389(1.06)	351559(0.13)
$4s4d \ ^1D_2$	379488	382023(0.67)	379276(0.06)
$4p4d \ ^3F_2^o$		468479	476801
$4p4d \ ^3F_3^o$		472174	480597
$4p4d \ ^3F_4^o$		476898	485492
$4p4d \ ^1D_2^o$		481577	488473
$4p4d \ ^3D_1^o$		497531	501724
$4p4d \ ^3D_2^o$		497123	501743
$4p4d \ ^3D_3^o$		499341	504993
$4p4d \ ^3P_0^o$		501757	506621
$4p4d \ ^3P_1^o$		502846	507395
$4p4d \ ^3P_2^o$		503754	508142

are suspect. The calculated $4p^3 \ ^2P_{3/2,1/2}^o$ levels deviate significantly, the $^2P_{3/2}^o$ by as much as 6000 cm^{-1} , from experiment. It is likely that these two levels are mistakenly inverted in the line identification. The experimental $4s4p4d \ ^2D_{3/2,5/2}^o$ levels deviate significantly from theory, and their line identifications are suspect.

In their CC study on low-energy electron collisions with magnesium, Bartschat *et al.* [27] noted that the quasi-two-electron system indeed possesses strong correlation effects in both the N -electron target and $(N+1)$ -electron collisional systems. Therefore they emphasized that it is absolutely essential to not rely on a target description with only good relative energies and oscillator strengths and that significant effort must be put into the optimization of the absolute energies using correlated orbitals with respect to the Mg^{2+} core. The effective many-body Hamiltonian based on the relativistic MR-MBPT theory accounts for both nondynamic and dynamic correlation corrections. Thus the method can account for the absolute energy difference between the N -electron target and $(N+1)$ -electron collisional systems. The experimental ionization energy $78.49 \pm 0.01 \text{ eV}$ is in very good agreement with the MR-MBPT theoretical prediction of 78.45 eV , reflecting the accuracy in the total energy difference between the Kr^{5+} and Kr^{6+} ions.

TABLE II. Comparison with experiment [47] of the calculated term energies (cm^{-1}) in galliumlike Kr (Kr^{5+}). Percentage deviations from experiment are given in parentheses.

State	Expt.	CAS-CI	MR-MBPT
$4s^2 4p^2 \ ^2P_{1/2}^o$	0	0	0
$4s^2 4p^2 \ ^2P_{3/2}^o$	8110	7598(6.31)	8157(0.58)
$4s 4p^2 \ ^4P_{1/2}$	107836	100979(6.36)	108238(0.37)
$4s 4p^2 \ ^4P_{3/2}$	111193	104080(6.40)	111574(0.34)
$4s 4p^2 \ ^4P_{5/2}$	115479	108262(6.25)	115880(0.35)
$4s 4p^2 \ ^2P_{3/2}$	141672	138325(2.36)	142067(0.28)
$4s 4p^2 \ ^2D_{5/2}$	142727	139304(2.40)	143093(0.26)
$4s 4p^2 \ ^2S_{1/2}$	170084	173014(1.72)	170203(0.07)
$4s 4p^2 \ ^2P_{1/2}$	180339	185151(2.67)	179705(0.35)
$4s 4p^2 \ ^2P_{3/2}$	183817	188949(2.79)	183299(0.28)
$4s^2 4d \ ^2D_{3/2}$	222122	224805(1.21)	222300(0.08)
$4s^2 4d \ ^2D_{5/2}$	223040	225432(1.07)	223183(0.06)
$4p^3 \ ^2D_{3/2}^o$	276011	269124(2.50)	277105(0.40)
$4p^3 \ ^2D_{5/2}^o$	278062	270541(2.70)	278870(0.29)
$4p^3 \ ^4S_{3/2}^o$	278787	275184(1.29)	278351(0.16)
$4p^3 \ ^2P_{3/2}^o$	303697	302986(0.23)	309344(1.86)
$4p^3 \ ^2P_{1/2}^o$	305385	301952(1.12)	303977(0.46)
$4s 4p 4d \ ^4P_{5/2}^o$	331956	325965(1.80)	332657(0.21)
$4s 4p 4d \ ^4P_{3/2}^o$	338032	332406(1.66)	338918(0.26)
$4s 4p 4d \ ^4P_{1/2}^o$	338364	331698(1.97)	338576(0.06)
$4s 4p 4d \ ^4D_{1/2}^o$	333936	328645(1.58)	334676(0.22)
$4s 4p 4d \ ^4D_{3/2}^o$	333133	327429(1.71)	333863(0.22)
$4s 4p 4d \ ^4D_{5/2}^o$	338119	332820(1.57)	339057(0.28)
$4s 4p 4d \ ^4D_{7/2}^o$	338447	332688(1.70)	338708(0.08)
$4s 4p 4d \ ^2D_{3/2}^o$	343190	340953(0.65)	343280(0.03)
$4s 4p 4d \ ^2D_{5/2}^o$	343505	341109(0.70)	343567(0.02)
$4s 4p 4d \ ^2F_{5/2}^o$	352547	350265(0.65)	352941(0.11)
$4s 4p 4d \ ^2F_{7/2}^o$	359035	352563(1.80)	357367(0.46)
$4s 4p 4d \ ^2P_{3/2}^o$	374279	380072(1.55)	374890(0.16)
$4s 4p 4d \ ^2P_{1/2}^o$	377255	382725(1.45)	378145(0.24)
$4s 4p 4d \ ^2D_{3/2}^o$	390595	401621(2.82)	394299(0.95)
$4s 4p 4d \ ^2D_{5/2}^o$	391878	402103(2.61)	394676(0.71)
$4s 4p 4d \ ^2P_{1/2}^o$		399488	393118
$4s 4p 4d \ ^2P_{3/2}^o$	393018	399844(1.74)	393494(0.12)
$4s 4p 4d \ ^2F_{7/2}^o$	398678	409489(2.71)	401011(0.59)
$4s 4p 4d \ ^2F_{5/2}^o$	399599	411090(2.88)	402159(0.64)

B. Electron-impact excitation cross sections

Figure 1 displays the electron-impact excitation cross sections for the $4s^2 \ ^1S \rightarrow 4s 4p \ ^3P$ excitation from 35-state CAS CI and effective many-body Hamiltonian *R*-matrix CC calculations. In the CC expansion, all 35 $n=4$ CAS CSFs in the target description and 149 CAS CSFs for the $(N+1)$ -electron bound channels were included. The contributions from each of the fine-structure levels $4s 4p \ ^3P_{2,1,0}^o$, as well as the sum of all individual contributions—the total cross section—from the effective Hamiltonian *R*-matrix calculation are displayed in the right four panels. The cross sections from the CAS CI

R-matrix calculations are given in the left panels for comparison. Convergence in the partial wave expansion occurs for summation up to $J=15/2$ in the *R*-matrix calculations. Calculations of the low-energy electron-impact excitation cross sections did not require the partial-wave summation to very high- J values. The electron impact excitations of the spin-forbidden $4s^2 \ ^1S \rightarrow 4s 4p \ ^3P$ transitions are dominated by resonances, as shown in earlier studies [25]. The excitation to the $4s 4p \ ^3P_1^o$ fine-structure level is the dominant excitation process near the threshold. The excitation to the $4s 4p \ ^3P_0^o$ fine-structure level, however, makes a substantial contribution, providing the threshold of the excitation process. Much of the computational effort went into mapping out the resonances. To resolve the resonances in the 1.0–1.35 Ry incident electron energy region, a very fine monotonic energy mesh of 2 meV was employed because the resonance region is crowded with very narrow and closely spaced resonances. With the fine energy mesh, we were able to resolve closely spaced resonances. The convoluted curves, however, did not show any noticeable difference.

A close examination of Fig. 1 reveals differences between the cross sections from the 35-state CAS-CI *R*-matrix calculations and those from the 35-state effective-Hamiltonian *R*-matrix calculations. The threshold resonances in the ≈ 1.1 Ry incident electron energy computed with the CAS-CI *R*-matrix method are uniformly shifted to lower energies, reflecting its failure to predict the $4s 4p \ ^3P_{2,1,0}^o$ energy levels accurately. The $4s 4p \ ^3P_{2,1,0}^o$ energies computed with the CAS CI are too low, by as much as 4000 cm^{-1} , compared with the experimental term energies, rendering determination of the resonance locations very inaccurate and unreliable. Therefore in an earlier study [25] it was necessary to repeat the CI-based *R*-matrix calculations a number of times, each time adjusting the separation between the threshold energies of the upper levels to which the strongest of these resonant states are attached. In marked contrast, the 35-state effective many-body Hamiltonian *R*-matrix CC calculations predict the Kr^{6+} and Kr^{5+} energy levels accurately, and thus provide accurate threshold resonances. The target energies from the effective Hamiltonian are of near spectroscopic accuracy, to within 200–400 cm^{-1} , and capable of predicting the excitation threshold to within 0.05 eV accuracy. There is also a significant difference in the excitation cross sections near the 1.10–1.20 Ry and in the 1.25–1.35 Ry regions. In the latter, the cross sections from the CAS CI *R*-matrix calculations are less pronounced than those computed with the effective-Hamiltonian *R*-matrix method. The resonance structures in the 1.10–1.20 Ry region are also significantly different between the two.

To investigate which groups of $4\ell 4\ell'$ target states contribute to the two major resonances centered within 1.1–1.2 Ry, *R*-matrix calculations were carried out by excluding several groups of target states. In the present study, the calculated total cross sections were convoluted with a 0.20 eV full width at half maximum (FWHM) Gaussian function to compare with the experimental data [6] as well as with the previous theoretical results [25]. For this purpose, 14- and 26-state *R*-matrix CC calculations were carried out in addition to the 35-state full CAS calculations. The 14-state CC expansion included the CSFs arising from the $4s^2$, $4s 4p$, $4p^2$, and

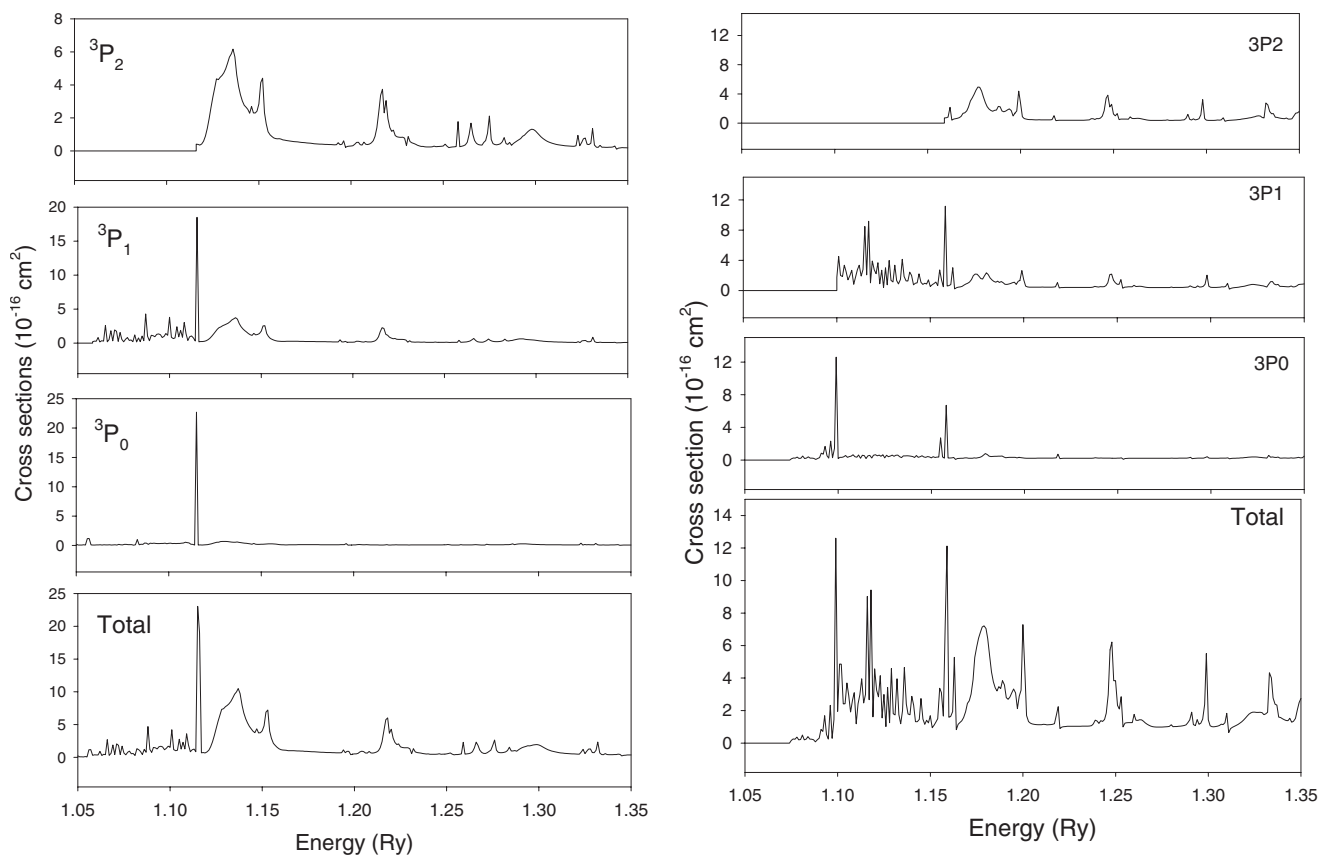


FIG. 1. Calculated electron-impact excitation cross section of the $4s^2\ ^1S_0-4s4p\ ^3P_{0,1,2}^o$ transition in Kr^{6+} . The cross sections in the left and right panels represent those computed by the CAS CI and the effective many-body Hamiltonian methods, respectively. The right panels show the total cross sections of electron-impact excitations to three $^3P^o$ fine-structure levels (top three panels on left).

$4s4d$ configurations and excluded a total of 12 states of the $4p4d$ and $4d^2$ configurations from the $n=4$ CAS. The 26-state CC expansion excludes only nine $4d^2$ CSFs. Figure 2 displays the three computed total cross sections from the diagonalization of the 35×35 and 149×149 CAS-CI matrices for the target and collisional systems, followed by the 14-, 26-, and 35-state R -matrix calculations. Each of the major resonances shown in the figure resulted from convolution over groups of resonances as can be seen by comparing Fig. 1 with Fig. 2. Figure 2 shows that the total cross sections from the 26-state and 35-state CAS-CI R -matrix calculations are nearly equal, indicating the convergence with respect to the CC expansion length. However, the converged cross sections have little resemblance to the experimental data.

The failure of the CAS-CI to predict the $4s4p\ ^3P_{2,1,0}^o$ energy levels accurately stems from its failure to account for valence-core correlation. A large-scale CI is a viable alternative to accurate prediction of the cross sections. Recent studies have employed a large-scale CI calculation that accounts for valence-core correlation to describe the resonant states more accurately: Recent Dirac R -matrix CC calculations [10,23,41] successfully employed large CI expansions, the Hamiltonian matrices of size $15\,266 \times 15\,266$ and larger, to predict strong resonances that appear in the electron impact excitations in Ne-like ions.

Figure 3 compares with experiment the three computed total cross sections from the diagonalization of the 35×35

and 149×149 effective many-body Hamiltonian matrices for the target and collisional systems, followed by the 14-, 26-, and 35-state R -matrix calculations. Experimental data points in Ref. [6] were shifted to the LS coupling energy $E_{av} = 15.297$ eV, neglecting the energy splitting of the $4s4p\ ^3P$ fine-structure levels to force the threshold to agree with the known spectroscopic value E_{av} . Therefore, in the present study, the experimental data points have been shifted to lower energy, by an amount 0.69 eV, to agree with the established $4s4p\ ^3P_0^o$ threshold energy where the onset of the excitation occurs. The upper resonance that appears between 1.15 and 1.20 Ry is dominated by the channels leading to $4s^2\ ^1S \rightarrow 4s4p\ ^3P_2^o$ excitation, and the lower one by those leading to $4s^2\ ^1S \rightarrow 4s4p\ ^3P_{0,1}^o$ excitations. The convoluted $4s^2\ ^1S-4s4p\ ^3P$ electron-impact excitation cross sections computed by using the 35-state effective Hamiltonian R -matrix CC are available as supplementary data in Ref. [48]. The figure shows that increasing CC expansion length leads to convergence toward the experimental data. The 35-state effective-Hamiltonian R -matrix CC calculations predict total cross sections in good agreement with experiment. All the features in the experimental cross section are reproduced well by the 35-state effective-Hamiltonian R -matrix CC calculations.

In an earlier work, Gorczyca *et al.* [25] calculated the electron-impact excitation cross sections for the $4s^2\ ^1S \rightarrow 4s4p\ ^3P$ transitions in Kr^{6+} using a 14-CSF CI followed

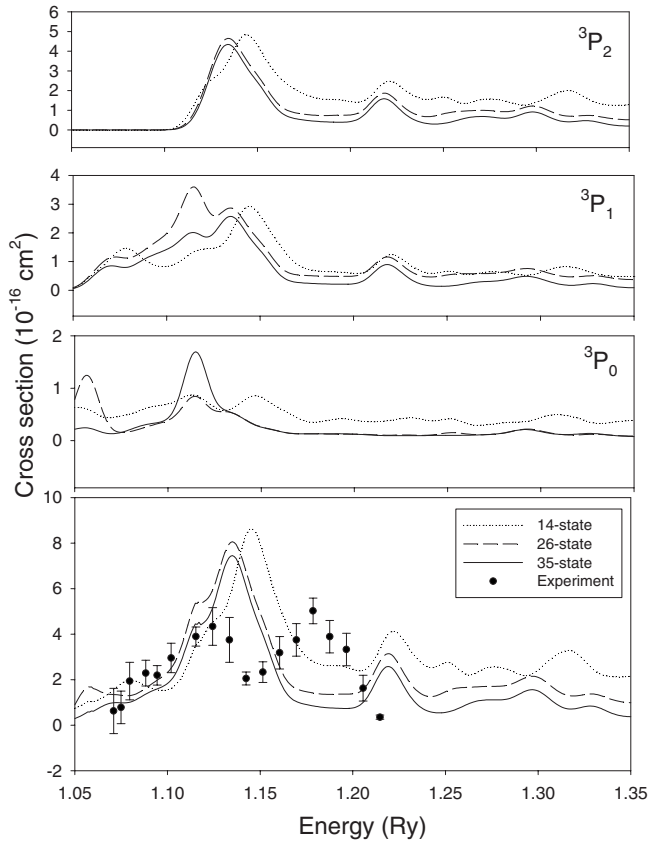


FIG. 2. Comparison with experiment of the electron-impact excitation cross sections for the $4s^2\ ^1S_0-4s4p\ ^3P_{0,1,2}^o$ excitations in Kr^{6+} computed by using the CAS-CI R -matrix CC method with increasing target-CSF expansion length. The upper three panels show the cross sections to three $^3P^o$ fine-structure levels. Solid, dashed, and dotted curves correspond, respectively, to 35-state, 26-state, and 14-state CC expansions. The values have been convoluted with a 0.20 eV FWHM Gaussian function. In the bottom panel, experimental cross section (filled circles) [6] is compared with the total cross sections of electron-impact excitations to three $^3P^o$ fine-structure levels shown in the upper panels. The experimental data points have been shifted to lower energy by 0.69 eV to agree with the $4s4p\ ^3P_0^o$ threshold energy.

by 5-, 8-, and 14-state R -matrix CC calculations. The total cross section (Fig. 4 in Ref. [25]), while the authors stated that the agreement with experiment is somewhat fortuitous, is similar to what we obtained from our 35-state effective Hamiltonian R -matrix calculation, including the sharp resonance feature near 1.18 Ry. Gorczyca *et al.* emphasized that the magnitude of these low-lying resonances are very sensitive to the interaction between the resonant states and that these interactions are dependent on the separation between resonances. This mandates accurate relativistic many-body calculations of the resonance contribution to the cross section. This is in contrast to the electron impact excitation of the $3s^2\ ^1S \rightarrow 3s3p\ ^1P$ transition in Mg-like ions, where the experimental total cross section [28] of this transition was readily reproduced by a 71-CSF CI followed by a 31-state R -matrix CC calculation [49]. The results obtained by Gorczyca *et al.* [25] explicate the potential sensitivity of R -matrix CC methods in calculating cross sections for electron impact

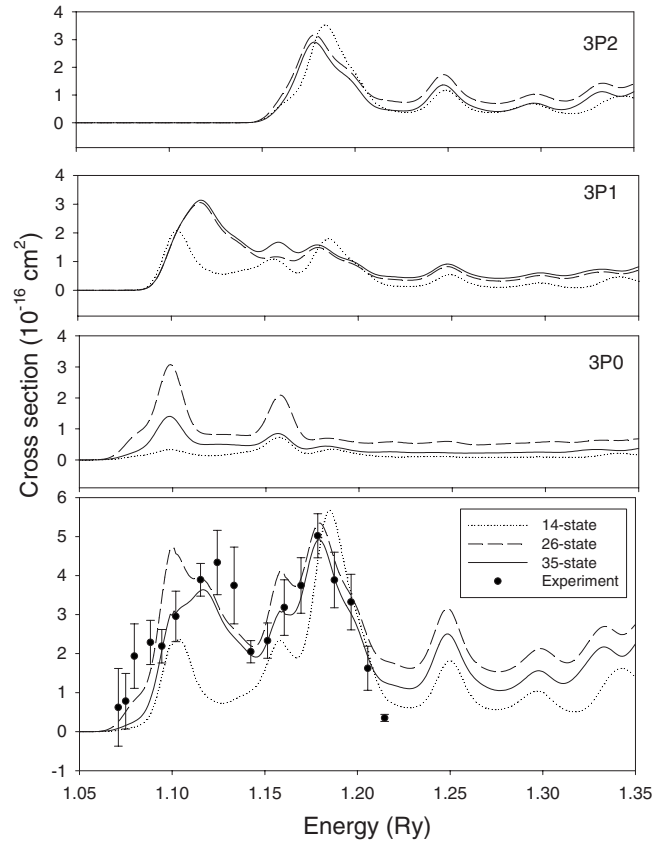


FIG. 3. Comparison with experiment of the electron-impact excitation cross sections for the $4s^2\ ^1S_0-4s4p\ ^3P_{0,1,2}^o$ excitations in Kr^{6+} computed by using the effective Hamiltonian R -matrix CC method with increasing target-CSF expansion length. The upper three panels show the cross sections to three $^3P^o$ fine-structure levels. Solid, dashed, and dotted curves correspond, respectively, to 35-state, 26-state, and 14-state CC expansions. The values have been convoluted with a 0.20 eV FWHM Gaussian function. In the bottom panel, experimental cross section (filled circles) [6] is compared with the total cross sections of electron-impact excitations to three $^3P^o$ fine-structure levels shown in the upper panels.

excitation of intercombination transitions where resonances play a dominant role in the excitation. Their work underscores the need for theoretical methods that determine resonance locations more accurately in order to improve the accuracy of the calculated cross sections. As the current study demonstrated, accurate description of valence-core correlation in both the N -electron target and the $(N+1)$ -electron collision systems is readily achieved by the effective many-body Hamiltonian, providing a framework for accurate determination of resonances.

IV. CONCLUSIONS

The electron impact excitation of the intercombination transition in Kr^{6+} is significantly more complicated than any of the systems previously studied because the large number of core electrons, the existence of a full $3d$ core in particular, with two valence electrons, makes it extremely difficult to accurately describe the target and resonance states. These

target and resonance levels have large level shifts due to relativistic many-body effects, which need to be fully incorporated to account for the nearly 1 eV fine structure splitting between the $4s4p\ ^3P_{2,1,0}^o$ as well as the relativistic many-body shifts in higher excited levels. As such, it provides a valuable benchmark to test a higher level of electron-atom collision theory.

In this study, the many-body theoretical underpinnings are brought to bear on the complex resonance processes in electron-impact excitation of the intercombination transition. The benchmark study exemplifies the importance of accurate representations of target and collisional states using methods that accurately account for static and dynamic correlations, as well as relativity. The effective Hamiltonian R -matrix CC provides accurate prediction of the cross sections for near-threshold electron impact excitations dominated by a large

number of resonance contributions, underscoring the importance of determining resonance locations by accurate relativistic many-body methods. The method refines its predecessor by providing a more accurate framework.

ACKNOWLEDGMENTS

One of the authors (Y.I.) gratefully acknowledges the Fondo Institucional para la Investigacion (FIPI) of the University of Puerto Rico (Grant No. 8-80-218) and the Lawrence Livermore National Laboratory (Subcontract No. B568401) for the support of this research. Y.I. thanks Dr. Beiersdorfer, Dr. M. F. Gu, and Dr. G. V. Brown (Lawrence Livermore National Laboratory) for valuable comments on the electron impact excitation cross sections.

-
- [1] P. Beiersdorfer, *Annu. Rev. Astron. Astrophys.* **41**, 343 (2003).
 [2] K. A. Berrington, C. P. Balance, D. C. Griffin, and N. R. Badnell, *J. Phys. B* **38**, 1667 (2005).
 [3] D. Post, J. Abdallah, R. Clark, and N. Putvinskaya, *Phys. Plasmas* **2**, 2328 (1995).
 [4] J. Rice, J. Terry, K. B. Fournier, M. Graf, M. Finkenthal, M. May, E. Marmor, W. Goldstein, and A. Hubbard, *J. Phys. B* **29**, 2191 (1996).
 [5] K. Fournier, D. Pacella, M. May, M. Finkenthal, and W. Goldstein, *Nucl. Fusion* **37**, 825 (1997).
 [6] M. E. Bannister, X. Q. Guo, T. M. Kojima, and G. H. Dunn, *Phys. Rev. Lett.* **72**, 3336 (1994).
 [7] S. J. Smith, J. A. Lozano, S. S. Tayal, and A. Chutjian, *Phys. Rev. A* **68**, 062708 (2003).
 [8] B. Wallbank, M. E. Bannister, H. F. Krause, Y.-S. Chung, A. C. H. Smith, N. Djuric, and G. H. Dunn, *Phys. Rev. A* **75**, 052703 (2007).
 [9] G. V. Brown, P. Beiersdorfer, H. Chen, J. H. Scofield, K. R. Boyce, R. L. Kelley, C. A. Kilbourne, F. S. Porter, M. F. Gu, S. M. Kahn, and A. E. Szymkowiak, *Phys. Rev. Lett.* **96**, 253201 (2006).
 [10] G. X. Chen, K. Kirby, E. Silver, N. S. Brickhouse, J. D. Gillaspay, J. N. Tan, J. M. Pomeroy, and J. M. Laming, *Phys. Rev. Lett.* **97**, 143201 (2006).
 [11] P. G. Burke, A. Hibbert, and W. D. Robb, *J. Phys. B* **4**, 153 (1971).
 [12] J.-J. Chang, *J. Phys. B* **8**, 2327 (1975).
 [13] K. L. Bell, P. G. Burke, and A. E. Kingston, *J. Phys. B* **10**, 3117 (1977).
 [14] N. S. Scott and P. G. Burke, *J. Phys. B* **13**, 4299 (1980).
 [15] P. G. Burke, K. A. Berrington, and C. V. Sukumar, *J. Phys. B* **14**, 289 (1981).
 [16] W. C. Fon and K. P. Lim, *J. Phys. B* **23**, 3691 (1990).
 [17] G. Kilgus, D. Habs, D. Schwalm, A. Wolf, R. Schuch, and N. R. Badnell, *Phys. Rev. A* **47**, 4859 (1993).
 [18] P. G. Burke and K. A. Berrington, *Atomic and Molecular Processes: An R-Matrix Approach* (IOP, Bristol, 1993).
 [19] R. Szymkowiak and J. Hinze, *J. Phys. B* **29**, 761 (1996).
 [20] T. J. M. Zouros, E. P. Benis, and T. W. Gorczyca, *Phys. Rev. A* **68**, 010701(R)(2003).
 [21] G. X. Chen and A. K. Pradhan, *Phys. Rev. Lett.* **89**, 013202 (2002).
 [22] M. Montenegro, W. Eissner, S. N. Nahar, and A. K. Pradhan, *J. Phys. B* **39**, 1863 (2006).
 [23] S. D. Loch, M. S. Pindzola, C. P. Ballance, and D. C. Griffin, *J. Phys. B* **39**, 85 (2006).
 [24] S. Hossain, S. S. Tayal, S. J. Smith, J. C. Raymond, and A. Chutjian, *Phys. Rev. A* **75**, 022709 (2007).
 [25] T. W. Gorczyca, M. S. Pindzola, N. R. Badnell, and D. C. Griffin, *Phys. Rev. A* **51**, 488 (1995).
 [26] M. J. Vilkas and Y. Ishikawa, *Phys. Rev. A* **72**, 032512 (2005).
 [27] K. Bartschat, O. Zatsarinsky, I. Bray, D. V. Fursa, and A. T. Stelbovics, *J. Phys. B* **37**, 2617 (2004).
 [28] Y.-S. Chung, N. Djuric, B. Wallbank, G. H. Dunn, M. E. Bannister, and A. C. H. Smith, *Phys. Rev. A* **55**, 2044 (1997).
 [29] V. A. Dzuba, V. V. Flambaum, and M. G. Kozlov, *Phys. Rev. A* **54**, 3948 (1996).
 [30] V. A. Dzuba, V. V. Flambaum, J. S. M. Ginges, and M. G. Kozlov, *Phys. Rev. A* **66**, 012111 (2002).
 [31] M. S. Safronova, W. R. Johnson, and U. I. Safronova, *Phys. Rev. A* **54**, 2850 (1996).
 [32] U. I. Safronova, C. Namba, J. R. Albritton, W. R. Johnson, and M. S. Safronova, *Phys. Rev. A* **65**, 022507 (2002).
 [33] I. M. Savukov and W. R. Johnson, *Phys. Rev. A* **65**, 042503 (2002).
 [34] M. J. Vilkas and Y. Ishikawa, *Phys. Rev. A* **68**, 012503 (2003).
 [35] M. J. Vilkas and Y. Ishikawa, *J. Phys. B* **37**, 1803 (2004).
 [36] P. H. Norrington and I. P. Grant, *J. Phys. B* **20**, 4869 (1987).
 [37] S. Ait-Tahar, I. P. Grant, and P. H. Norrington, *Phys. Rev. A* **54**, 3984 (1996).
 [38] M. J. Vilkas and Y. Ishikawa, *Phys. Rev. A* **75**, 062508 (2007).
 [39] J. Sucher, *Phys. Rev. A* **22**, 348 (1980).
 [40] M. H. Mittleman, *Phys. Rev. A* **24**, 1167 (1981).
 [41] G. X. Chen, K. Kirby, and N. S. Brickhouse, *Phys. Rev. A* **73**, 052708 (2006).
 [42] C. Møller and M. S. Plesset, *Phys. Rev.* **46**, 618 (1934).
 [43] M. J. Vilkas and Y. Ishikawa, *Phys. Rev. A* **69**, 062503 (2004).
 [44] V. Kvasnicka, *Czech. J. Phys., Sect. B* **25**, 371 (1975).

- [45] Y. Ishikawa, H. M. Quiney, and G. L. Malli, *Phys. Rev. A* **43**, 3270 (1991).
- [46] P. Indelicato, O. Gorceix, and J. P. Desclaux, *J. Phys. B* **20**, 651 (1987).
- [47] J. R. Fuhr *et al.*, "NIST Atomic Spectra Database" Ver. 3.1.00, NIST Physical Reference Data. Available online at <http://physics.nist.gov/PhysRefDat/ASD/index.html>
- [48] See EPAPS Document No. E-PLRAAN-77-014805 for the table of convoluted electron-impact excitation cross sections. For more information on EPAPS, see <http://www.aip.org/pubservs/epaps.html>.
- [49] T. Kai, R. Srivastava, and S. Nakazaki, *Phys. Rev. A* **70**, 062705 (2004).